

# Bifurcations analysis of the twist-Fréedericksz transition in a nematic liquid-crystal cell with pre-twist boundary conditions: the asymmetric case

FERNANDO P. DA COSTA<sup>1,2</sup>, MARIA ISABEL MÉNDEZ<sup>3</sup> and JOÃO T. PINTO<sup>4</sup>

<sup>1</sup>*Departamento de Ciências e Tecnologia, Universidade Aberta, Rua da Escola Politécnica 141–147, 1269-001 Lisboa, Portugal*

<sup>2</sup>*Center for Mathematical Analysis, Geometry and Dynamical Systems, Instituto Superior Técnico, Universidade de Lisboa, Av. Rovisco Pais, 1049-001 Lisboa, Portugal  
email: fcosta@uab.pt*

<sup>3</sup>*Departamento de Matemáticas, IES Antonio López García, Calle Arquitectos 39, 28903 Getafe, Madrid, Spain  
email: misabel.mendezaller@educa.madrid.org*

<sup>4</sup>*Department of Mathematics and Center for Mathematical Analysis, Geometry and Dynamical Systems, Instituto Superior Técnico, Universidade de Lisboa, Av. Rovisco Pais, 1049-001 Lisboa, Portugal  
email: jpinto@math.tecnico.ulisboa.pt*

(Received 10 December 2015; revised 13 May 2016; accepted 18 May 2016; first published online 16 June 2016)

In the paper, *Bifurcation analysis of the twist-Fréedericksz transition in a nematic liquid-crystal cell with pre-twist boundary conditions* (2009 *Eur. J. Appl. Math.* **20**, 269–287) by da Costa *et al.* the twist-Fréedericksz transition in a nematic liquid-crystal one-dimensional cell of length  $L$  was studied, imposing an antisymmetric net twist Dirichlet condition at the cell boundaries. In the present paper, we extend that study to the more general case of net twist Dirichlet conditions without any kind of symmetry restrictions. We use phase-plane analysis tools and appropriately defined time maps to obtain the bifurcation diagrams of the model when  $L$  is the bifurcation parameter, and related these diagrams with the one in the antisymmetric situation. The stability of the bifurcating solutions is investigated by applying the method of Maginu (1978 *J. Math. Anal. Appl.* **63**, 224–243).

**Key words:** Twist-Fréedericksz transition, Liquid-crystal cells, Non-homogeneous Dirichlet two-point boundary value problems, Bifurcation of equilibria

## 1 Introduction

In the operation of liquid-crystal devices, the phenomena of Fréedericksz transitions in nematic liquid-crystal cells are of paramount technological importance [8, Chapter 5] and give rise to interesting and challenging mathematical problems [7, Section 3.4].

A nematic liquid-crystal cell is basically a thin layer (a few microns) of a nematic liquid-crystal held between two glass plates whose inner surfaces are chemically treated in such a way as to force a certain alignment (anchoring) of the rod like nematic

liquid-crystal molecules lying close to the cell boundaries. This surface alignment induces an alignment in the liquid-crystal molecules filling the cell bulk so that the total free energy is minimized.

When an exterior electric or magnetic field is applied to the cell a competition takes place between the reorienting effects of the field and the alignment imposed by the surface anchoring. Minimization of the total free energy (field, elastic bulk, and anchoring) then forces a realignment of the molecules in the cell bulk (and, in the case of the so called weak anchoring conditions, also of those at the cell surface [2]) when the field intensity increases above a threshold value dependent on the physico-chemical characteristics of the device. This bifurcation phenomenon is called Fréedericksz transition, after the Soviet physicist who discovered it [4].

If we model the rod-like nematic liquid-crystal molecules by a “director vector field”  $\mathbf{n} = \mathbf{n}(\mathbf{x})$ , with  $\|\mathbf{n}\| \equiv 1$ , a system with strong anchoring of the molecules at the cell surface occupying a region  $\Omega$  has a total free energy of the director field given by

$$\int_{\Omega} w(\mathbf{n}, \nabla \mathbf{n}) d\mathbf{x},$$

where the free-energy density  $w$  embodies the competition between the energy cost of distortions of the director field versus the energy reduction associated with aligning parallel (or perpendicular) to the magnetic field, and is given by

$$2w = K_1 (\operatorname{div} \mathbf{n})^2 + K_2 (\mathbf{n} \cdot \operatorname{curl} \mathbf{n})^2 + K_3 \|\mathbf{n} \times \operatorname{curl} \mathbf{n}\|^2 - \mu_0 \Delta \chi (\mathbf{H} \cdot \mathbf{n})^2,$$

where  $K_1$ ,  $K_2$ , and  $K_3$  are phenomenological elastic constants,  $\mu_0$  is the free-space magnetic permeability,  $\Delta \chi = \chi_{\parallel} - \chi_{\perp}$  is the difference between the diamagnetic susceptibilities parallel to versus perpendicular to the director, and  $\mathbf{H}$  is the (constant) applied magnetic field. See, e.g., [7].

We consider the geometry of the twist-Fréedericksz transition, with an asymmetric pre-twist at the boundary. Thus, we consider a thin slab of nematic liquid-crystal bounded by two parallel planes a distance  $d$  apart from each other, unbounded and extending to infinity in any direction parallel to these planes. Define a positively oriented orthogonal coordinate system  $(x, y, z)$  such that  $z$  is perpendicular to the bounding planes. Let the director field be represented by

$$\mathbf{n} = (\cos \phi(z, \tau), \sin \phi(z, \tau), 0), \quad (1.1)$$

where  $\phi$  denotes the (twist) angle of the director. We will assume that in the liquid-crystal cell the director is fixed in opposing orientations  $-\phi_0$  and  $\phi_1$  at the two opposing planes bounding the device in the  $z$  direction. This induces a net twist of the director vector field  $\mathbf{n}$  across the cell (see Figure 1).

We will consider a magnetic vector field  $\mathbf{H}$  applied along the constant direction  $(0, 1, 0)$  with intensity  $H = \|\mathbf{H}\|$  and are interested in studying the effect it induces in the stationary director distribution, according to the Ericksen–Leslie theory [7].

In terms of the angle representation 1.1, the simplest model for the dynamics of the director field in the absence of flow is the gradient flow on the *free energy* of the system and, in dimensionless form, the initial-boundary value problem governing the behaviour

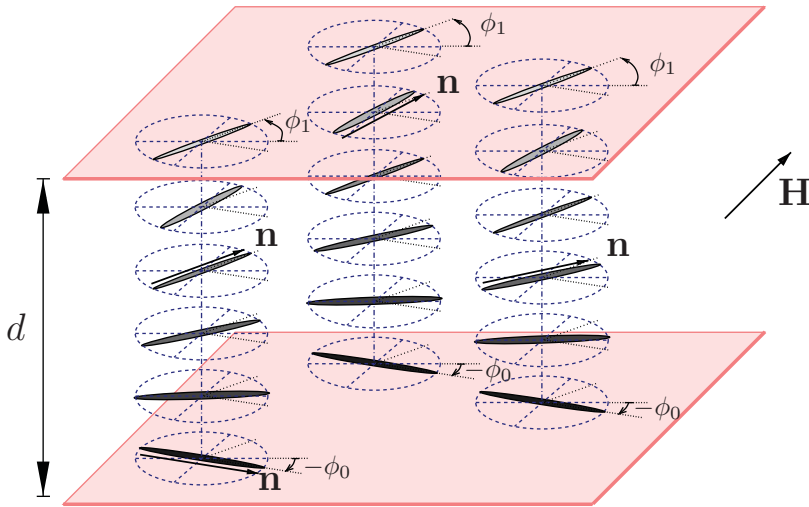


FIGURE 1. Geometry of the liquid-crystal cell with asymmetric pre-twist. The director  $\mathbf{n}$  orientation inside the cell corresponds to the situation in branch  $C_r$  (with  $k = 0$ ) in Section 3.1 below.

of the director field is then

$$\frac{\partial \phi}{\partial s} = \frac{\partial^2 \phi}{\partial \zeta^2} + \lambda \sin \phi \cos \phi, \quad (s, \zeta) \in \mathbb{R}^+ \times (0, 1) \tag{1.2}$$

$$\phi(\cdot, 0) = -\phi_0, \quad \phi(\cdot, 1) = \phi_1, \tag{1.3}$$

$$\phi(0, \cdot) = \phi_{\text{initial}} \tag{1.4}$$

where

$$s := \frac{K_2}{\gamma_1 d^2} \tau, \quad \zeta := \frac{z}{d}, \quad \lambda := \frac{\mu_0 \Delta \chi H^2 d^2}{K_2}, \tag{1.5}$$

with all the material parameters positive for our system of interest. Observe that the dimensionless control parameter  $\lambda$  is proportional to the square of the magnetic field strength.

The associated equilibrium problem is given by

$$\frac{d^2 \phi}{d\zeta^2} + \lambda \sin \phi \cos \phi = 0, \quad 0 < \zeta < 1 \tag{1.6}$$

$$\phi(0) = -\phi_0, \quad \phi(1) = \phi_1. \tag{1.7}$$

In the classical twist-Fréedericksz-transition problem, we have  $\phi_0 = \phi_1 = 0$ , the system possesses a simple symmetry,  $\phi(\zeta) \leftrightarrow -\phi(\zeta)$ , and the ground-state solution ( $\phi = 0$ , which is invariant under this symmetry) loses stability to a pair of symmetric solutions at a pitchfork bifurcation at  $\lambda_c = \pi^2$ .

In da Costa *et al.* [1] a system with antisymmetric pre-twist ( $\phi_0 = \phi_1 \neq 0$ ) was studied. We no longer have the simple symmetry above. The problem still possesses  $\mathbb{Z}_2$  symmetry, however it is now of the form  $\phi(\zeta) \leftrightarrow -\phi(1 - \zeta)$ . The ground-state solution (which is invariant under this symmetry) is no longer uniform. The problem still has a classical pitchfork bifurcation diagram, with the symmetric solution branch bifurcating at a value

$\lambda_c$ , which is necessarily greater than  $\pi^2$ , as was showed in da Costa et al. [1]. Observe that the antisymmetric nature of the boundary data is crucial to this scenario.

In the present paper, we consider the asymmetric case ( $\phi_0 \neq \phi_1$ , both non-zero). We conclude that no pitchfork bifurcation points remain: the pitchforks that had not been broken in the passage from the classical twist cenario to the antisymmetric one are now broken when the  $\phi_0$  becomes different from  $\phi_1$ , and the result is a bifurcation diagram with only saddle-node bifurcation points, branches emanating from them, and single non-bifurcating branch of solutions.

The approach will be based on the time maps and phase-plane methods developed in da Costa et al. [1] for the antisymmetric case. The stability of these branches is also studied by applying the results of Maginu [6], also based on the behaviour of time maps, which allows the classification of the stationary solution branches as stable, asymptotically stable, or unstable. A more detailed study of the stability indices of the equilibria and the characterization of their connecting orbits will be the subject of a future paper.

### 2 Preliminaries

We will be concerned with the stationary solutions to (1.2)–(1.4), i.e., solutions of (1.6), (1.7). Consider the change of variables  $t = t(\zeta) := \sqrt{\frac{\lambda}{2}} (\zeta - \frac{1}{2})$ , and let  $\zeta(t)$  be its inverse function. Let

$$L := \sqrt{\frac{\lambda}{8}}. \tag{2.1}$$

Then,  $\phi(\zeta)$  is a solution of (1.6), (1.7) iff  $x(t) := \phi(\zeta(t))$  is a solution of

$$\begin{cases} x' = y \\ y' = -\sin 2x \end{cases} \tag{2.2}$$

$$x(-L) = -\phi_0, \quad x(L) = \phi_1, \tag{2.3}$$

where  $\phi_0, \phi_1 \in (0, \frac{\pi}{2})$ , and  $(t, x, y) \in [-L, L] \times [-\pi/2, \pi/2] \times \mathbb{R}$ . The bifurcation parameter is now  $L > 0$ . Note that  $L \propto H$ . We shall treat the independent variable  $t$  in (2.2), (2.3) as the “time” of the dynamical system associated with (1.2). Note that this “time” corresponds to the original spacial variable  $\zeta$  and not to the original time  $s$ .

The study of the bifurcation structure of solutions to (2.2)–(2.3) when  $\phi_0 = \phi_1$  was done in da Costa et al. [1]. We now consider the general case, where no relation between the values of  $\phi_0$  and  $\phi_1$  is imposed. As in da Costa et al. [1], we shall use the tools of time maps and phase-plane analysis.

The phase portrait of (2.2) is presented in Figure 2.

For studying solutions to (2.2), (2.3) we need to consider some time maps measuring the time spent by the orbits. These maps are easily obtained from the fact that (2.2), (2.3) is a conservative system with energy

$$V(x, y) = y^2 - \cos 2x, \tag{2.4}$$

which means that its orbits are subsets of the level sets of this function.

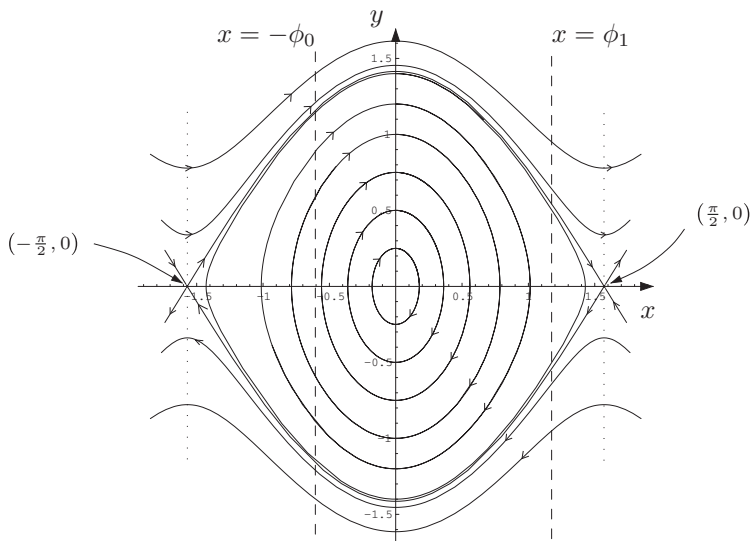


FIGURE 2. Orbits of (2.2) with the Dirichlet boundary condition (2.3) marked by the dashed vertical lines (with  $0 < \phi_0 < \phi_1 < \pi/2$ ).

Let  $\alpha \in (0, \frac{\pi}{2})$  and denote by  $\gamma_\alpha$  the orbit that, at time  $t = 0$ , intersects the  $x$ -axis at  $(\alpha, 0)$ . Clearly  $\gamma_\alpha$  is a periodic orbit (cf. Figure 2). Let  $P(\alpha)$  be its period and define

$$T(\alpha) := \frac{1}{4}P(\alpha) = \int_0^\alpha \frac{dx}{\sqrt{\cos 2x - \cos 2\alpha}}, \tag{2.5}$$

where the second equality arises from the symmetry of the system with respect to reflexions in the  $x$ - and  $y$ -axis. Thus,  $T(\alpha)$  is the time it takes for the point of intersection of  $\gamma_\alpha$  with the  $y$ -axis (which, by conservation of  $V$  along orbits, we easily conclude to be the point  $(0, \beta)$  with  $\beta = \sqrt{2} \sin \alpha$ ) to reach the  $x$ -axis (at the point  $(\alpha, 0)$ , by construction).

As in da Costa *et al.* [1], two other time maps will be needed. The time map

$$T_1(\alpha, \phi) := \int_0^\phi \frac{dx}{\sqrt{\cos 2x - \cos 2\alpha}}, \tag{2.6}$$

measures the time spent from the point of intersection of the orbit  $\gamma_\alpha$  with the  $y$ -axis to reach the line  $x = \phi \leq \alpha$ . Clearly  $T_1(\phi, \phi) = T(\phi)$ . We will also consider a map  $T_2$  analogous to  $T_1$  but relevant for orbits crossing the  $y$ -axis on or above the heteroclinic orbit  $\gamma_h$  connecting  $(-\pi/2, 0)$  to  $(\pi/2, 0)$ , i.e., at a point  $(0, \beta)$  with  $\beta \geq \sqrt{2}$ , namely

$$T_2(\beta, \phi) := \int_0^\phi \frac{dx}{\sqrt{\beta^2 + \cos 2x - 1}}. \tag{2.7}$$

We can continuously extend this map to values  $\beta < \sqrt{2}$  by  $T_2(\beta, \phi) := T_1(\alpha(\beta), \phi)$ , where  $\alpha(\beta)$  is defined to be the unique value of  $\alpha$  for which the points  $(\alpha, 0)$  and  $(0, \beta)$  are on the same orbit. Since the orbits are contained in the level sets of  $V$ , a brief inspection of Figure 2 allows us to conclude that  $\beta \mapsto \alpha(\beta)$  is a monotonically increasing function and

thus, for each fixed  $\phi$ , there is a smaller  $\beta$  for which  $T_2(\beta, \phi)$  is defined which is the value  $\beta_\phi$  for which  $(\beta_\phi, 0)$  and  $(\phi, 0)$  are on the same orbit. For  $\beta$  below  $\beta_\phi$  no orbit satisfies the boundary condition at  $t = L$ .

Our analysis depends heavily on the following monotonicity properties of the time maps defined above. A proof of these results can be checked in da Costa et al. [1].

**Proposition 1** *Let  $\alpha \in (0, \frac{\pi}{2})$ ,  $\phi \in (0, \alpha)$ , and  $\beta \geq \beta_\phi$ . Then,*

- (1) *the time-map  $T : (0, \frac{\pi}{2}) \rightarrow (0, +\infty)$  defined by (2.5) is strictly increasing and converges to  $\frac{\pi}{2\sqrt{2}}$  as  $\alpha \rightarrow 0$ , and to  $+\infty$  as  $\alpha \rightarrow \frac{\pi}{2}$ .*
- (2) *for each fixed  $\phi$  the time maps  $T_1(\cdot, \phi)$  and  $T_2(\cdot, \phi)$ , defined by (2.6) and (2.7), respectively, are strictly decreasing. The same holds for  $T_2(\cdot, \frac{\pi}{2})$ .*

### 3 Bifurcation analysis

The study of (2.2), (2.3) in the antisymmetric case  $\phi_0 = \phi_1$  was done in da Costa et al. [1] and will serve as a guide to our present study. In the antisymmetric case, a special role is played by the solutions of (2.2), (2.3) that additionally satisfy the homogeneous Neumann boundary condition  $y(-L) = y(L) = 0$  (note that  $y = x'$ ). The values of  $L$  for which these solutions occur were termed “critical” (cf. [1, Figure 4 and Table 1]) and are pitchfork bifurcation points of the system [1, Figure 9]. The orbits corresponding to these values of  $L$  were denoted by  $\gamma^*$ .

Due to the symmetry of the vector field of (2.2) and the asymmetry of the boundary condition (2.3) there are no solutions to (2.2), (2.3) satisfying homogeneous Neumann boundary conditions at both  $t = -L$  and  $t = L$ . However, there are solutions that satisfy such a condition at one, or the other, of the end points of the time interval. Although these do not correspond to bifurcation solutions, and the corresponding values of  $L$  are not bifurcation points of (2.2), (2.3), they are important solutions that help us to organize the information and construct the bifurcation diagram in the asymmetric case, and relate it to the antisymmetric case already studied.

The two asymmetric cases  $\phi_0 < \phi_1$  and  $\phi_0 > \phi_1$  give rise to different bifurcation diagrams and will be studied separately below. Since the approach for both cases is the same, we will present the first one in a more detailed way, and for the second will just briefly refer to the corresponding results.

#### 3.1 Case $\phi_0 < \phi_1$

##### 3.1.1 The “critical” cases

Let  $\gamma_*$  be the orbit of (2.2), (2.3) that satisfies the additional homogeneous Neumann condition  $y(L) = 0$ . See Figure 3(a). It is clear from this figure and from the definition of the time maps in the previous section that the time spent by  $\gamma_*$  is  $T_* := T(\phi_1) + T_1(\phi_1, \phi_0)$ . Since the total time spent by every orbit is  $2L$ , the corresponding half-length  $L$  is  $L_* = \frac{1}{2}T_*$ .

In a similar way, the orbit that satisfies the homogeneous Neumann boundary condition  $y(-L) = 0$  will be denoted by  $\gamma^*$ . See Figure 3(b). The time spent in by this orbit is  $T^* := 3T(\phi_1) - T_1(\phi_1, \phi_0)$ , and the corresponding half-length of the interval is  $L^* = \frac{1}{2}T^*$ .

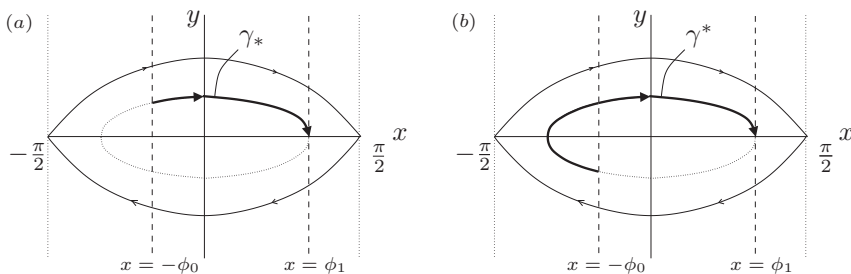


FIGURE 3. Two “critical” orbits of (2.2), (2.3) with  $\phi_0 < \phi_1$ : (a)  $\gamma_*$  when  $2L = T_* := T(\phi_1) + T_1(\phi_1, \phi_0)$ ; (b)  $\gamma^*$  when  $2L = T^* := 3T(\phi_1) - T_1(\phi_1, \phi_0)$ .

From the definitions of the time maps we easily observe that

$$T_* = T(\phi_1) + T_1(\phi_1, \phi_0) < 2T(\phi_1) < 3T(\phi_1) - T_1(\phi_1, \phi_0) = T^*, \tag{3.1}$$

and these the inequalities turn to equalities if  $\phi_0 = \phi_1$ , which, as already pointed out, was the case considered in da Costa *et al.* [1].

By analogy to the terminology used in da Costa *et al.* [1] for the antisymmetric case, we shall call these solutions, orbits, etc., “critical”, although, as we shall see, they do not correspond to any critical feature in the bifurcation diagrams. However, they will be very useful for the remaining constructions. In particular, as a matter of terminology and when appropriate, we will keep denoting by subcritical [resp., supercritical] those situations with values of  $L$  smaller [resp., larger] than  $L^*$  ou  $L_*$ .

### 3.1.2 The subcritical case relative to $\gamma_*$

By Proposition 1, it is clear that the function  $(\phi_1, \frac{\pi}{2}) \ni \alpha \mapsto T_A(\alpha) := T_1(\alpha, \phi_1) + T_1(\alpha, \phi_0)$  is monotonically decreasing and  $T_A(\alpha) \uparrow T_*$  as  $\alpha \downarrow \phi_1$ . The corresponding orbit of (2.2), (2.3) is a subset of the level set  $V(\alpha, 0)$  of  $V$ . Since the time it spends is  $2L = T_A(\alpha) < T_*$ , we call it subcritical relative to  $\gamma_*$ . Using the relation between the time maps  $T_1$  and  $T_2$ , we can extend this approach to orbits intersecting the  $y$ -axis above the heteroclinic orbit  $\gamma_h$ . The time taken by these orbits is also smaller than  $T_*$  and decreases as the ordinate of the intersection point increases.

In Figure 4, we present two of these orbits subcritical relative to  $\gamma_*$ , together with the critical orbit  $\gamma_*$ . The monotonicity of the time maps imply that, for each  $L \in (0, \frac{1}{2}T_*)$  there is a single subcritical solution to (2.2), (2.3).

### 3.1.3 The supercritical case relative to $\gamma_*$

Consider again  $\alpha \in (\phi_1, \frac{\pi}{2})$  and the level set  $V(\alpha, 0)$  of  $V$ . For  $\alpha > \phi_1$  but close to  $\phi_1$ , we take an orbit of (2.2), (2.3) close to  $\gamma_*$  which has its end point with  $y(L) < 0$ , as presented in Figure 5. A brief inspection of this figure allows us to conclude that the time spent by this orbit is  $T_C(\alpha) := 2T(\alpha) + T_1(\alpha, \phi_0) - T_1(\alpha, \phi_1)$ . (The notation  $T_{C_r}$  was used in da Costa *et al.* [1] for a branch of solutions with a given symmetry relative to the origin. We use the same notation here because our  $C_r$  solutions will coincide with those of that

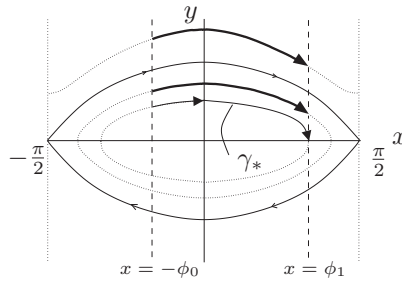


FIGURE 4. Two orbits of (2.2), (2.3), with  $\phi_0 < \phi_1$ , subcritical relative to the orbit  $\gamma_*$ .

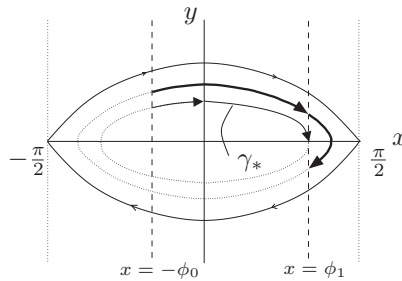


FIGURE 5. An orbit of (2.2), (2.3), with  $\phi_0 < \phi_1$ , supercritical relative to the orbit  $\gamma_*$ .

paper when  $\phi_0 = \phi_1$ ; the same will be done for other solution branches further down the paper.) Clearly,  $T_{C_r}(\alpha) \rightarrow T_*$  as  $\alpha \rightarrow \phi_1$ .

We shall prove that  $T_{C_r}(\alpha) > T_*$  for  $\alpha > \phi_1$ , thus providing a justification for calling these orbits supercritical relative to  $\gamma_*$ . From the expression of  $T_{C_r}$  and Proposition 1 we conclude that

$$\frac{dT_{C_r}}{d\alpha}(\alpha) = T'(\alpha) + \frac{\partial T_1}{\partial \alpha}(\alpha, \phi_0) - \frac{\partial T_1}{\partial \alpha}(\alpha, \phi_1) > \frac{\partial T_1}{\partial \alpha}(\alpha, \phi_0) - \frac{\partial T_1}{\partial \alpha}(\alpha, \phi_1). \tag{3.2}$$

To obtain the sign of the right-hand side observe that

$$\frac{\partial}{\partial \phi} \frac{\partial T_1}{\partial \alpha} = \frac{\partial}{\partial \alpha} \frac{\partial T_1}{\partial \phi} = \frac{\partial}{\partial \alpha} \frac{1}{\sqrt{\cos 2\phi - \cos 2\alpha}} = -\frac{\sin 2\alpha}{(\cos 2\phi - \cos 2\alpha)^{3/2}} < 0.$$

From this inequality and the assumption that  $\phi_0 < \phi_1$  we infer that

$$\frac{\partial T_1}{\partial \alpha}(\alpha, \phi_0) > \frac{\partial T_1}{\partial \alpha}(\alpha, \phi_1),$$

and plugging this into (3.2) gives that  $T_{C_r}$  is strictly increasing with  $\alpha$ , concluding the proof.

### 3.1.4 The supercritical case relative to $\gamma_*$

Consider an orbit in  $V(\alpha, 0)$ , with  $\alpha \in (\phi_1, \frac{\pi}{2})$ , as represented in Figure 6(a). From this figure and the definition of the time maps we immediately conclude that the time spent



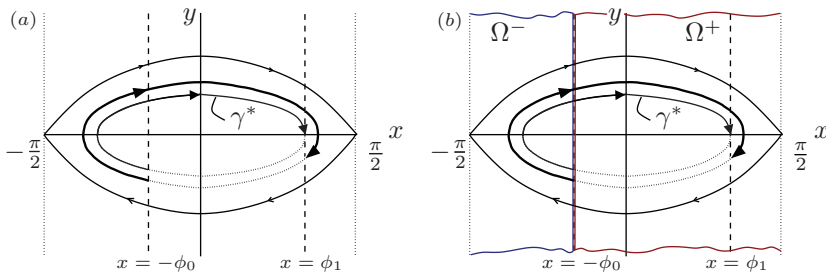


FIGURE 6. (a) An orbit of (2.2), (2.3), with  $\phi_0 < \phi_1$ , supercritical relative to the orbit  $\gamma^*$ .  
 (b) The  $\Omega^-$  and  $\Omega^+$  regions.

to travel this orbit is  $T_D(\alpha) := 4T(\alpha) - T_1(\alpha, \phi_0) - T_1(\alpha, \phi_1)$  (see subsection 3.1.3 for a justification of this notation).

Clearly  $T_D(\alpha) \rightarrow T_*$  as  $\alpha \rightarrow \phi_1$ . We shall prove that  $T_D(\alpha) > T_*$ . In order to prove this, consider the strips  $\Omega^- := (-\pi/2, -\phi_0) \times \mathbb{R}$ , and  $\Omega^+ := [-\phi_0, \pi/2) \times \mathbb{R}$ . Let  $\gamma^{*\pm} := \gamma^* \cap \Omega^\pm$ . Denoting by  $D$  an orbit of the type represented in Figure 6, let also  $D^\pm = D \cap \Omega^\pm$ . Since  $\gamma^{*+} = \gamma_*$ , the time spent in  $\gamma^{*+}$  is equal to  $T_*$ .

Thus, in  $\Omega^+$  we just need to compare  $T_*$  with the time spent by  $D^+$ . But  $D^+$  is really an orbit of type  $C_r$  with  $\alpha > \phi_1$  and thus, by the previous subsection,  $T_{D^+}(\alpha) > T_*$ .

In  $\Omega^-$  we need to compare the time taken by the orbit  $D^-$  with that taken by  $\gamma^{*-}$ , which a brief inspection to Figure 6(b) shows it is equal to  $2T(\phi_1) - 2T_1(\phi_1, \phi_0)$ . Since

$$T_{D^-}(\alpha) = 2T(\alpha) - 2T_1(\alpha, \phi_0), \quad \alpha \in (\phi_1, \pi/2),$$

we have  $\frac{dT_{D^-}}{d\alpha}(\alpha) = 2T'(\alpha) - 2\frac{\partial T_1}{\partial \alpha}(\alpha, \phi_0)$ , and the monotonicity results in Proposition 1 imply that this derivative is positive, and thus  $T_{D^-}(\alpha) > 2T(\phi_1) - 2T_1(\phi_1, \phi_0)$ .

Finally, from the above we have

$$\begin{aligned} T_D(\alpha) &= T_{D^-}(\alpha) + T_{D^+}(\alpha) \\ &> 2T(\phi_1) - 2T_1(\phi_1, \phi_0) + T_* = 3T(\phi_1) - T_1(\phi_1, \phi_0) \\ &= T_*, \end{aligned}$$

as we wanted to prove.

### 3.1.5 The subcritical case relative to $\gamma^*$

To complete the analysis, let us consider orbits in  $V(\alpha, 0)$ , with  $\alpha \in (\phi_1, \frac{\pi}{2})$ , as represented in Figure 7.

It is clear from this plot that the time spent by this orbit is  $T_{C_r}(\alpha) := 2T(\alpha) - T_1(\alpha, \phi_0) + T_1(\alpha, \phi_1)$  (see subsection 3.1.3 for a justification of this notation  $T_{C_r}$ ).

It is also clear that  $T_{C_r}(\alpha) \rightarrow T_*$  as  $\alpha \rightarrow \phi_1$ . We shall prove that, for  $\alpha > \phi_1$  sufficiently close to  $\phi_1$ , we have  $T_{C_r}(\alpha) < T_*$ . This is not as easy to prove as in the previous cases. We start by considering in (2.5) and (2.6) a new variable  $\tilde{\alpha} := \sin^2 \alpha$ , and changing in (2.5)

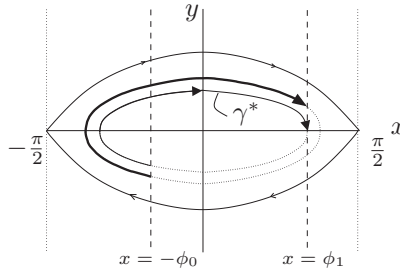


FIGURE 7. An orbit of (2.2), (2.3), with  $\phi_0 < \phi_1$ , subcritical relative to the orbit  $\gamma^*$ .

the integration variable  $x \mapsto \theta$  where  $\sin x = \sqrt{\tilde{\alpha}} \sin \theta$ . This allows us to write

$$T_{C_\ell}(\alpha) = \tilde{T}_{C_\ell}(\tilde{\alpha}) := \sqrt{2} \int_0^{\pi/2} \frac{d\theta}{\sqrt{1 - \tilde{\alpha} \sin^2 \theta}} + \frac{1}{\sqrt{2}} \int_{\phi_0}^{\phi_1} \frac{dx}{\sqrt{\tilde{\alpha} - \sin^2 x}}, \tag{3.3}$$

Differentiating we obtain

$$\frac{d\tilde{T}_{C_\ell}}{d\tilde{\alpha}} = \frac{1}{\sqrt{2}} \int_0^{\pi/2} \frac{\sin^2 \theta}{(1 - \tilde{\alpha} \sin^2 \theta)^{3/2}} d\theta - \frac{1}{2\sqrt{2}} \int_{\phi_0}^{\phi_1} \frac{dx}{(\tilde{\alpha} - \sin^2 x)^{3/2}},$$

and computing the second derivative we obtain

$$\frac{d^2 \tilde{T}_{C_\ell}}{d\tilde{\alpha}^2} = \frac{3}{2\sqrt{2}} \int_0^{\pi/2} \frac{\sin^4 \theta}{(1 - \tilde{\alpha} \sin^2 \theta)^{5/2}} d\theta + \frac{3}{4\sqrt{2}} \int_{\phi_0}^{\phi_1} \frac{dx}{(\tilde{\alpha} - \sin^2 x)^{5/2}} > 0.$$

Hence,  $\tilde{T}_{C_\ell}$  is a convex function of  $\tilde{\alpha} := \sin^2 \alpha \in (\sin^2 \phi_1, 1)$ . From the definition of  $T_{C_\ell}$  and  $\tilde{T}_{C_\ell}$ , the above expressions, and Proposition 1, we also conclude that  $\tilde{T}_{C_\ell} \rightarrow +\infty$  as  $\tilde{\alpha} \rightarrow 1$ , and  $\frac{d\tilde{T}_{C_\ell}}{d\tilde{\alpha}} \rightarrow -\infty$  as  $\tilde{\alpha} \rightarrow \sin^2 \phi_1$ ; however, note that  $\tilde{T}_{C_\ell} \rightarrow T^*$  as  $\tilde{\alpha} \rightarrow \sin^2 \phi_1$  (see the start of this paragraph).

This behaviour obviously implies the existence of a single local extrema (a minimum) of  $\tilde{T}_{C_\ell}$ , and hence of  $T_{C_\ell}$ , in the interior of their respective intervals of definition, and thus  $T_{C_\ell}(\alpha) < T^*$  when  $\alpha > \phi_1$  sufficiently close to  $\phi_1$ . This justifies us calling this situation a (local) subcritical case relative to  $\gamma^*$ . We emphasize that the situation is *local*: if  $\alpha$  is larger than the minimizer of  $T_{C_\ell}(\alpha)$ , the value of this function increases without bound as  $\alpha \rightarrow \pi/2$ , and thus at some point, it will certainly be larger than  $T^*$ .

Collecting the results obtained in the subsections 3.1.1–3.1.5, we obtain the bifurcation diagram in Figure 8. Note that, due to the symmetry of the system, the value of  $y(-L)$  of the orbits  $\gamma_*$  and  $\gamma^*$  have the same absolute value (and different signs).

### 3.1.6 Other solution branches

In addition to the solution branches studied above and represented in Figure 8, (2.2)–(2.3) has an infinite number of solution families, each corresponding to orbits circling the

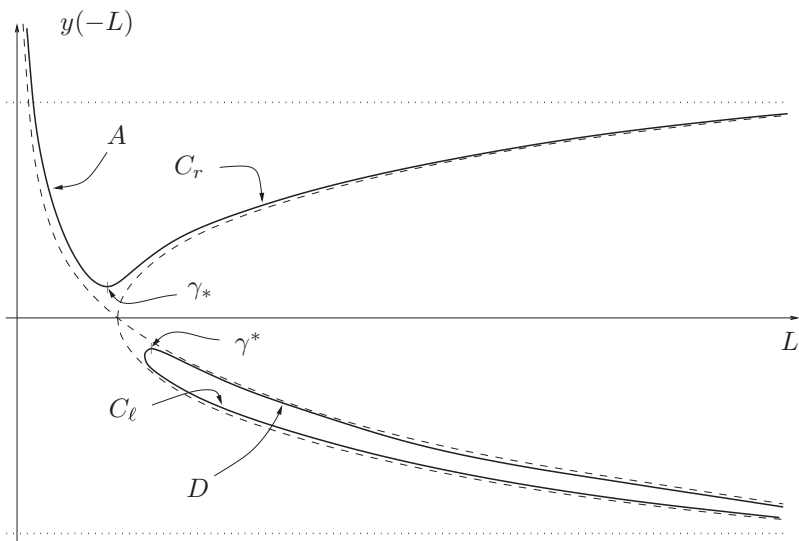


FIGURE 8. Solid lines: portion of the bifurcation diagram when  $\phi_0 < \phi_1$  constructed from the analysis of the time maps about  $\gamma_*$  and  $\gamma^*$  presented in subsections 3.1.1–3.1.5. Dashed lines: the corresponding diagram when  $\phi_0 = \phi_1$  (from da Costa *et al.* [1]). The designation of the orbits by letters  $A$ ,  $C_\ell$ ,  $C_r$ , and  $D$  correspond to those used in da Costa *et al.* [1]: see Table 1 and Figure 8 of that article.

origin a complete  $k$  number of times ( $k = 1, 2, \dots$ ). As in the cases studied above, it is convenient to start by considering orbits corresponding to solutions that satisfy the additional boundary condition  $y(L) = 0$ , and, as before, we denote those orbits by a star, in this case by  $\gamma_{*k}$  and  $\gamma_k^*$ . Although they do not correspond to bifurcating points, they are very useful in organizing our knowledge about the solution branches. In Table 1, we present the orbit  $\gamma_{*k}$  and those which form a connected branch with it when  $L$  changes from the value corresponding to  $\gamma_{*k}$ . In Table 2, we present the analogous picture concerning the orbit  $\gamma_k^*$ .

Observe that these orbits are analogous to those studied in the previous subsections, which can be considered the case  $k = 0$  in this description (i.e., the orbits do not complete a full turn around the origin). The amounts of time spent by each of these orbits are exactly those of the corresponding ones in subsections 3.1.1–3.1.5 with the addition of  $4kT(\alpha)$ , which is the time of  $k$  full turns about the origin.

The following conclusions are easily drawn:

- (a) From the definitions of the time maps it follows that  $T_k^*(\phi_1) < T_{(k+1)*}(\phi_1)$ .
- (b) From (3.1), we immediately get  $T_{k*}(\phi_1) < T_k^*(\phi_1)$ .
- (c) From the results in subsections 3.1.3 and 3.1.4 and the fact that the time spent by the orbits with  $k > 0$  is equal to the time spent by those with  $k = 0$  plus  $4kT(\alpha)$ , we easily conclude that  $T_{C_r}(\alpha) > T_{*k}(\phi_1)$  and  $T_D(\alpha) > T_k^*(\phi_1)$ .
- (d) The study of the relation between  $T_{C_\ell}(\alpha)$  and  $T_k^*(\phi_1)$ , for  $\alpha > \phi_1$  sufficiently close to  $\phi_1$  proceeds exactly as in subsection 3.1.5, paying attention to the fact that we need to add  $4kT(\alpha)$  to those computations. Since  $T'(\alpha) \rightarrow T(\phi_1) \in (0, +\infty)$  as  $\alpha \downarrow \phi_1$ , and

Table 1. Branch of solutions to (2.2), (2.3), with  $\phi_0 < \phi_1$ , winding  $k$  full times around  $\mathbf{0}$  and containing the solution  $\gamma_{*k}$ . (For  $k = 0$  the portion of the orbits with a thin trace should be disregarded)

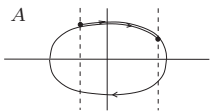
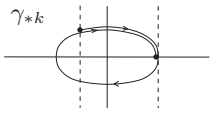
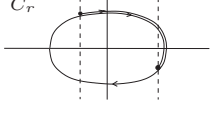
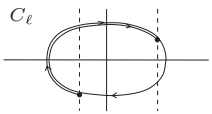
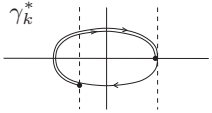
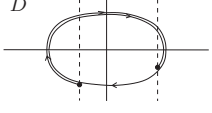
Orbit $\gamma_{\alpha,k}$ (winds $k$ times around $\mathbf{0}$ )	Time taken by the orbit $\gamma_{\alpha,k}$
 <p>A</p>	$T_A(\alpha) := 4kT(\alpha) + T_1(\alpha, \phi_0) + T_1(\alpha, \phi_1)$
 <p><math>\gamma_{*k}</math></p>	$T_{*k}(\phi_1) := (4k + 1)T(\phi_1) + T_1(\phi_1, \phi_0)$
 <p><math>C_r</math></p>	$T_{C_r}(\alpha) := (4k + 2)T(\alpha) + T_1(\alpha, \phi_0) - T_1(\alpha, \phi_1)$

Table 2. Branch of solutions to (2.2), (2.3), with  $\phi_0 < \phi_1$ , winding  $k$  full times around  $\mathbf{0}$  and containing the solution  $\gamma_k^*$ . (For  $k = 0$  the portion of the orbits with a thin trace should be disregarded)

Orbit $\gamma_{\alpha,k}$ (winds $k$ times around $\mathbf{0}$ )	Time taken by the orbit $\gamma_{\alpha,k}$
 <p><math>C_l</math></p>	$T_{C_l}(\alpha) := (4k + 2)T(\alpha) - T_1(\alpha, \phi_0) + T_1(\alpha, \phi_1)$
 <p><math>\gamma_k^*</math></p>	$T_k^*(\phi_1) := (4k + 3)T(\phi_1) - T_1(\phi_1, \phi_0)$
 <p>D</p>	$T_D(\alpha) := 4(k + 1)T(\alpha) - T_1(\alpha, \phi_0) - T_1(\alpha, \phi_1)$

$\tilde{T}''(\tilde{\alpha}) > 0$ , the addition of  $4kT(\alpha)$  to the right-hand side of (3.3) does not change the conclusion. Hence, we have  $T_{C_l}(\alpha) < T_k^*(\phi_1)$ , for  $\alpha - \phi_1 > 0$  sufficiently small. Also, the other conclusions inferred from the convexity of  $\tilde{\alpha} \mapsto \tilde{T}_{C_l}(\tilde{\alpha})$  remain valid.

(e) Finally, it remains to study the relation between  $T_A(\alpha)$  and  $T_{*k}(\phi_1)$ . The analysis also follows that presented in subsection 3.1.5. Changing variables as in subsection 3.1.5,

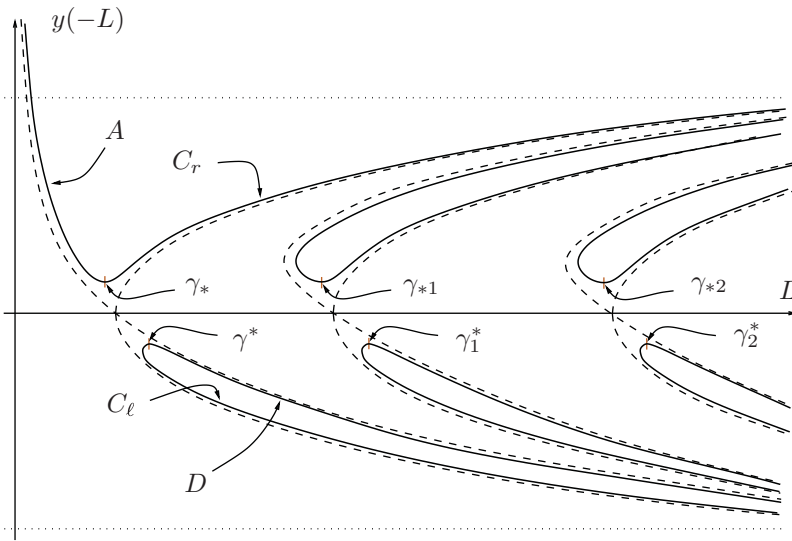


FIGURE 9. Solid lines: portion of the bifurcation diagram when  $\phi_0 < \phi_1$  constructed from the analysis presented in subsections 3.1.1–3.1.6. Dashed lines: the corresponding diagram when  $\phi_0 = \phi_1$  (from da Costa *et al.* [1]). The designation of the orbits by letters  $A$ ,  $C_l$ ,  $C_r$  and  $D$  correspond to those used in da Costa *et al.* [1]: see Table 1 and Figure 8 of that article.

we can write an expression for  $T_A(\alpha)$  similar to (3.3), namely

$$T_A(\alpha) = \tilde{T}_A(\tilde{\alpha}) := 2\sqrt{2}k \int_0^{\pi/2} \frac{d\theta}{\sqrt{1 - \tilde{\alpha} \sin^2 \theta}} + \frac{1}{\sqrt{2}} \int_0^{\phi_0} \frac{dx}{\sqrt{\tilde{\alpha} - \sin^2 x}} + \frac{1}{\sqrt{2}} \int_0^{\phi_0} \frac{dx}{\sqrt{\tilde{\alpha} - \sin^2 x}}.$$

Now, the convexity argument employed in subsection 3.1.5 and also used in case **d** above, can again be applied to conclude that, for  $\alpha - \phi_1 > 0$  sufficiently small, type  $A$  orbits satisfy  $T_A(\alpha) < T_{*k}(\phi_1)$  and the corresponding branch in the diagram  $L$  vs.  $y(-L)$  is convex. Note that, in contrast to the case studied in subsection 3.1.5, but as was the case in da Costa *et al.* [1], the branches of type  $A$  solutions have a (unique, by convexity) saddle-node, since we know that, from Proposition 1,  $T_A(\alpha) \rightarrow +\infty$  as  $\alpha \rightarrow \frac{\pi}{2}$ .

Thus, we conclude from these results that, for each  $k$ , the relation of the various types of orbits among themselves is the same as existed in the case  $k = 0$  illustrated in Figure 8. We collect the results obtained thus far in the bifurcation diagram of Figure 9. Observe that, due to the symmetry of the system, the value of  $y(-L)$  of the orbits  $\gamma_{*k}$  are the same for all  $k$ , and the same happens for  $\gamma_k^*$ ; as was the case when  $k = 0$ , for all  $k$  these values in  $\gamma_{*k}$  and in  $\gamma_k^*$  have the same absolute value (and different signs).

### 3.2 Case $\phi_0 > \phi_1$

The analysis of the case  $\phi_0 > \phi_1$  proceeds in a way entirely similar to the case  $\phi_0 < \phi_1$  and so we will not present the details of the arguments in what follows. We will, in the

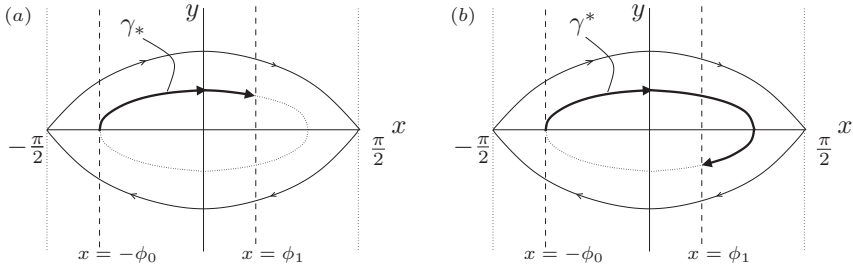


FIGURE 10. Two “critical” orbits of (2.2), (2.3) with  $\phi_0 > \phi_1$ : (a)  $\gamma_*$  when  $2L = T_* := T(\phi_1) + T_1(\phi_1, \phi_0)$ ; (b)  $\gamma_*$  when  $2L = T^* := 3T(\phi_1) - T_1(\phi_1, \phi_0)$ .

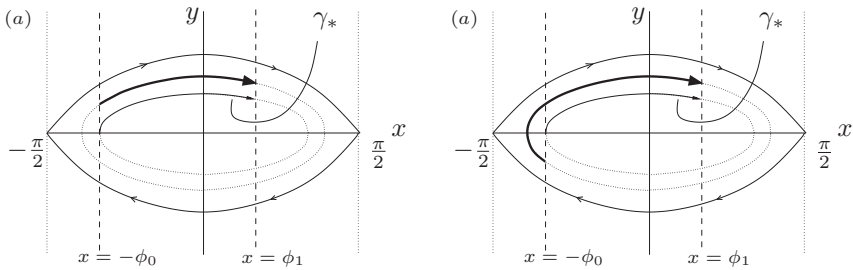


FIGURE 11. Orbits of (2.2), (2.3), with  $\phi_0 > \phi_1$  which are: (a) subcritical relative to the orbit  $\gamma_*$ ; (b) supercritical relative to the orbit  $\gamma_*$ .

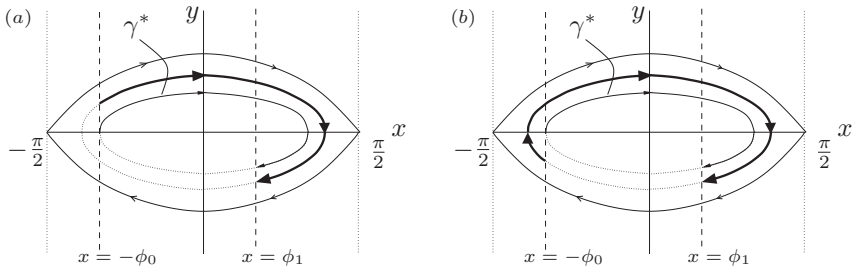


FIGURE 12. Orbits of (2.2), (2.3), with  $\phi_0 > \phi_1$  which are: (a) subcritical relative to the orbit  $\gamma_*$  (for  $\alpha - \phi_0 > 0$  sufficiently small); (b) supercritical relative to the orbit  $\gamma_*$ .

next figures, exhibit the plots of the several types of orbits and the bifurcation diagram obtained. We start, in Figure 10, with the orbits that, at  $t = -L$ , satisfy the additional boundary condition  $y(-L) = 0$ , which we designate by “critical” orbits, as done in the similar situation in subsection 3.1.1.

Due to the symmetry of the problem relative to the transformations  $x \mapsto -x$  and  $\phi_0 \leftrightarrow \phi_1$ , we conclude that from each “critical” orbit emerges two branches, a subcritical and a supercritical one, with exactly the same properties as obtained for the corresponding branches in subsections 3.1.2–3.1.5. These orbits are illustrated in Figures 11 and 12.

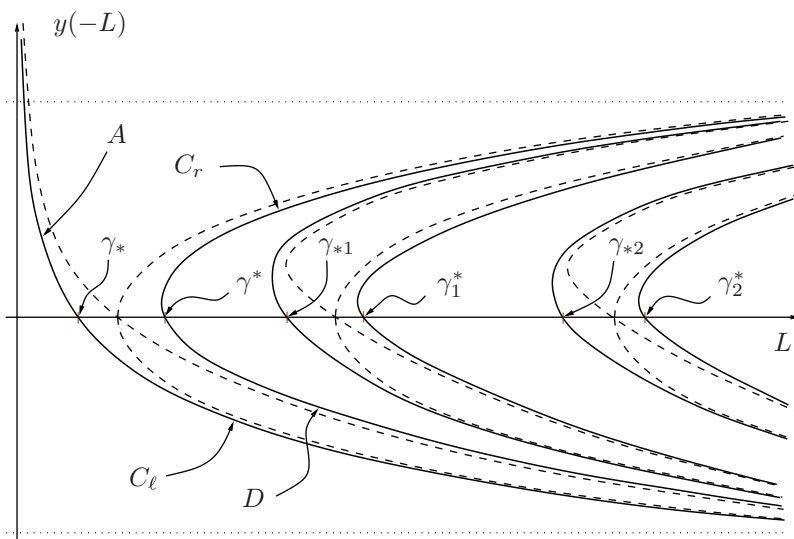


FIGURE 13. Solid lines: portion of the bifurcation diagram when  $\phi_0 > \phi_1$  constructed from what was presented and discussed in subsection 3.2. Dashed lines: the corresponding diagram when  $\phi_0 = \phi_1$  (from da Costa *et al.* [1]). The designation of the orbits by letters  $A$ ,  $C_l$ ,  $C_r$ , and  $D$  correspond to those used in da Costa *et al.* [1]: see Table 1 and Figure 8 of that article.

In an entirely analogous way to what was presented in Section 3.1.6, we also have the solution branches corresponding to orbits circling the origin a complete number  $k \geq 1$  of turns.

Collecting these results, we can plot the bifurcation diagram corresponding to the case  $\phi_0 > \phi_1$ . This is done in Figure 13. To understand the apparently drastic difference relative to the diagram for the case  $\phi_0 < \phi_1$  presented in Figure 9 we need to bear in mind the fact that in *both* cases what is being plotted in the vertical axis is the value of  $y(-L)$  of the corresponding orbit. If, in the case  $\phi_0 > \phi_1$ , we choose to plot the value of  $y(L)$  instead, by the symmetry considerations alluded to above, the corresponding bifurcation diagram will be equal to that of Figure 9.

#### 4 Stability analysis of the equilibria

In this section, we present a brief study of the stability of the equilibria using the approach of Maginu [6]. We believe it is possible, by a modification to methods originally developed for homogeneous Neumann boundary conditions (see, e.g., [3] and [5, Section 4.3]) to provide more detailed information about the *unstable* solutions, in particular clarifying, for each unstable equilibrium, which directions are unstable, and to characterize their heteroclinic connections. This will be postponed to a later work.

We classify as stable, asymptotically stable, or unstable the branches of equilibria determined in the last section. The results of Maginu [6] relevant to our case are the Theorems 3.1–3.3. What the first two of these theorems state is that solutions  $(x(t), y(t))$  of (2.2)–(2.3) are asymptotically stable as stationary solutions of the corresponding partial

differential equation (1.2)–(1.4) if  $y(t)$  has no zeros in  $[-L, L)$  or in  $(-L, L]$ ; and are unstable if  $y(t)$  has two or more zeros.

Clearly, these results take care of the stability characterization of all the branches of solutions with  $k \geq 1$  (they are all unstable), and also when  $k = 0$  of the branch denoted by  $A$  (which is asymptotically stable), and by  $D$  (which is unstable).

Theorem 3.3 of Maginu [6] is one of a series of results characterizing the case when  $y(t)$  has a single zero in  $[-L, L]$ , located in  $(-L, L)$ . Maginus' result states that such an equilibrium  $E$  is asymptotically stable if the corresponding time map  $T_E(\alpha)$  is strictly increasing, and is unstable if it is strictly decreasing.

Applied to our case, this result will allow us to determine the stability of the remaining cases, namely: the branches  $C_r$  and  $C_\ell$  when  $k = 0$ .

Consider  $\phi_0 < \phi_1$ . Let us start with the  $C_r$  branch. Clearly such solutions are of the type considered in Maginu [6, Theorem 3.3] (the existence of a single time instant for which  $y(t) = 0$ ). In Subsection 3.1.3, we concluded that  $\frac{dT_{C_r}}{d\alpha} > 0$ . Hence, Maginu's result imply the branch is asymptotically stable.

Let us consider now the case of the  $C_\ell$  branch. The relevant computations are the ones in subsection 3.1.5, where we concluded that  $T_{C_\ell}(\alpha)$  is convex, with a single local minimum. This means that  $\frac{dT_{C_\ell}}{d\alpha} < 0$  for the part of the  $C_\ell$  branch to the left of the  $\gamma^*$  and to the right of the leftmost point of the branch, i.e., the saddle-node bifurcation point (which corresponds to the orbit for which  $T_{C_\ell}(\alpha)$  attains its unique minimum.) So, by Maginu [6, Theorem 3.3], these equilibria are unstable. For the remaining part of the  $C_\ell$  branch, i.e., for points of the orbit below the saddle-node bifurcation point, we have  $\frac{dT_{C_\ell}}{d\alpha} > 0$ , and thus, again by Maginu [6, Theorem 3.3], the corresponding equilibria are asymptotically stable.

These stability conclusions for the  $k = 0$  branches are collected in Figure 14.

Exactly the same results can be applied to the case when  $\phi_0 > \phi_1$  with analogous results: by Theorems 3.1 and 3.2 of Maginu [6] all the  $k \geq 1$  branches are unstable, as well as the  $D$  branch, whereas the  $A$  branch is asymptotically stable. An analysis corresponding to that in subsections 3.1.3 and 3.1.5 and the application of theorem 3.3 of Maginu [6] results in the conclusion that  $C_\ell$  is an asymptotically stable branch, and the portion of the  $C_r$  branch between  $\gamma^*$  and the leftmost point (a saddle-node) of the branch corresponds to unstable equilibria, whereas the points above this last point are asymptotically stable equilibria.

These conclusions about the stability of the  $k = 0$  branches are collected in Figure 15.

## 5 Conclusions

In this paper, we study a model for the twist-Fréedericksz transition in a nematic liquid-crystal cell with pre-twist at the boundary.

The case of an antisymmetric pre-twist (the director alignment angle at opposing sides of the cell boundary have the same absolute value  $\phi_0$  but opposite signs) was studied in da Costa et al. [1] where it was shown that the bifurcation diagram occurring in the case without pre-twist (which is just a non-linear pendulum equation with homogeneous Dirichlet conditions  $\phi_0 = 0$  at the boundary) is modified such that all the even numbered pitchfork bifurcations are broken and saddle-node points appear in their stead. The



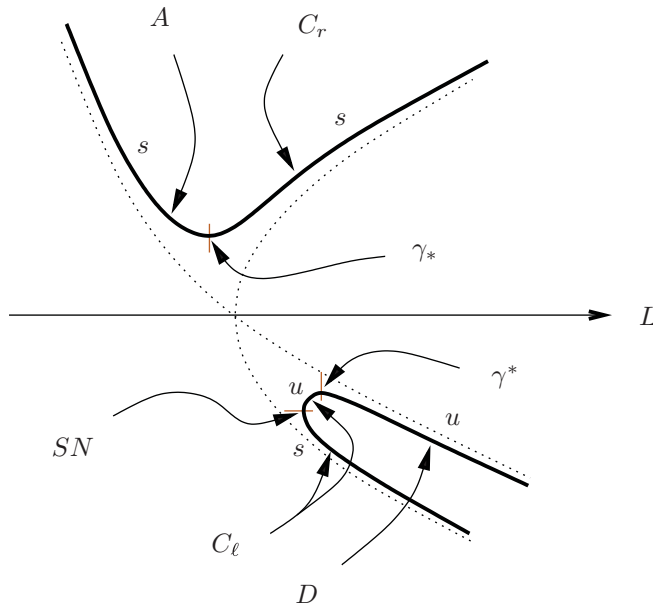


FIGURE 14. Enlargement of the bifurcation diagram of Figure 8. The saddle-node bifurcation point referred to in the text is denoted by *SN*, and the letters *s* and *u* denote branches of stable and unstable solutions, respectively. The remaining notation is as in Figure 8.

odd-numbered pitchforks remain unbroken, occurring at an higher field value than in the absence of pre-twist. For instance, the first bifurcation point now occurs at a magnetic field value  $H_c \propto \sqrt{\lambda_c}$  where  $\lambda_c \approx \pi^2(1 + \frac{1}{2}\phi_0^2)$ , for small values of the pre-twist  $\phi_0$ .

We complement the antisymmetric study in da Costa *et al.* [1] by considering the more general asymmetric case where the opposing sides of the cell boundary have fixed director angles  $-\phi_0 < 0$  and  $\phi_1 > 0$ , with different absolute values. This condition leads to the breakup of those pitchfork bifurcations that remained in the antisymmetric case, so that the system bifurcation diagram now consists in a series of saddle-note bifurcations. The first saddle-node always occurs at a larger magnetic field value  $H \propto L$  than the first pitchfork bifurcation magnetic field value in the antisymmetric case,  $H_c$  (cf. Figures 14 and 15.)

A stability study of the bifurcating branches as stationary solutions to the partial differential equation (1.2)–(1.4) is done using the method in Maginu [6]. We conclude that stable solutions are those corresponding to the non-bifurcating branch containing the monotonic increasing solutions at small magnetic field (denoted by *A* in Sections 3 and 4), as well as one of the bifurcating branches from the first saddle-node.

In order to fully understand the dynamics of (1.2)–(1.4), an important feature is the analysis of the heteroclinic connections between stationary solutions. We expect to proceed with these studies in the future.

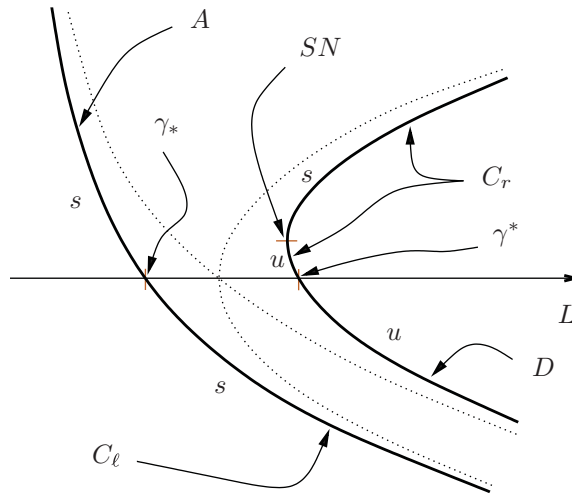


FIGURE 15. Enlargement of the bifurcation diagram of Figure 13. The saddle-node bifurcation point referred to in the text is denoted by  $SN$ , and the letters  $s$  and  $u$  denote branches of stable and unstable solutions, respectively. The remaining notation is as in Figure 13.

### Acknowledgements

F.P. da C. and J.T.P. were partially supported by FCT/Portugal through UID/MAT/04459/2013. Parts of Section 3.1 first appeared in the dissertation submitted by M.I.M to the *Universidad Nacional de Educación a Distancia*, Madrid, Spain, in June 2014, as part of the requirements for the degree of *Máster en Matemáticas Avanzadas*.

### References

- [1] DA COSTA, F. P., GARTLAND, JR., E. C., GRINFELD, M. & PINTO, J. T. (2009) Bifurcation analysis of the twist-Fréedericksz transition in a nematic liquid-crystal cell with pre-twist boundary condition. *Eur. J. Appl. Math.* **20**, 269–287.
- [2] DA COSTA, F. P., GRINFELD, M., MOTTRAM, N. & PINTO, J. T. (2009) Uniqueness in the Freedericksz transition with weak anchoring. *J. Differ. Equ.* **246**, 2590–2600.
- [3] FIEDLER, B. & ROCHA, C. (1996) Heteroclinic orbits of semilinear parabolic equations. *J. Differ. Equ.* **125**(1), 239–281.
- [4] FREEDERICKSZ, V. & ZOLINA, V. (1929) On the use of a magnetic field in the measurement of the forces tending to orient an anisotropic liquid in a thin homogeneous layer. *Trans. Am. Electrochem. Soc.* **55**, 85–96.
- [5] HALE, J. K. (1988) *Asymptotic Behavior of Dissipative Systems*, Mathematical Surveys and Monographs, Vol. 25, American Mathematical Society, Providence, RI.
- [6] MAGINU, K. (1978) Stability of stationary solutions of a semilinear parabolic partial differential equation. *J. Math. Anal. Appl.* **63**, 224–243.
- [7] STEWART, I. W. (2004) *The Static and Dynamic Continuum Theory of Liquid Crystals*, The Liquid Crystals Book Series, Vol. 2, Taylor & Francis, London.
- [8] YANG, D.-K. & WU, S.-T. (2015) *Fundamentals of Liquid Crystal Devices*, 2nd ed., Wiley-SID Series in Display Technology, John Wiley & Sons, Chichester.